AIAA JOURNAL
Vol. 44, No. 3, March 2006

Variable Turbulent Schmidt-Number Formulation for Scramjet Applications

X. Xiao,* J. R. Edwards,† and H. A. Hassan‡
North Carolina State University, Raleigh, North Carolina 27695-7910
and
A. D. Cutler§
George Washington University, Hampton, Virginia 23668

A new turbulence model suited for calculating the turbulent Schmidt number as part of the solution is presented. The model is based on a set of two equations: one governing the sum of the variances of mass fractions and the other governing its dissipation rate. The model is used to study mixing in the absence of reactions. Its predictions are compared with two sets of experiments involving supersonic mixing. The first involves a coaxial jet: the center flow consists of a 95% He and 5% O_2 mixture at Mach 1.8, whereas the surrounding flow consists of air at Mach 1.8. The second involves mixing of H_2 at Mach 1.0 with vitiated N_2 at Mach 2.44. Local turbulent Schmidt numbers as low as 0.16 in the boundary region are computed. The results suggest that the choice of the turbulent Prandtl number is case dependent. In general, good agreement with experiment is indicated.

Nomenclature

$C_Y, C_{Y1} - C_{Y7}$	=	model constants
D	=	diffusion coefficient
k	=	turbulence kinetic energy
P	=	pressure
Pr	=	Prandtl number
Sc	=	Schmidt number
T	=	temperature
u_i	=	velocity
Y	=	mass fraction
ε_Y	=	dissipation rate of enthalpy variance
ζ	=	enstrophy
ν	=	kinematic viscosity
ρ	=	density
σ_Y	=	summation of mass fraction variance

Subscripts

m	=	species
t	=	turbulent
0	=	stagnation conditions

I. Introduction

In high-speed engines, thorough turbulent mixing of fuel and air is required to obtain high performance and high efficiency of combustion. Thus, the ability to predict turbulent mixing is crucial in obtaining accurate numerical simulation of engine performance. Current state of the art in computational fluid dynamics (CFD) simulation is to use traditional turbulence models that explicitly consider velocity fluctuations. As a result, both the turbulent Prandtl and Schmidt numbers are assumed constants. However, because the mixing of fuel and oxidizer is inversely proportional to the turbulent Schmidt number, a value of, say, 0.45 for the Schmidt number will produce twice as much diffusion as that with a value of 0.9. Eklund et al.[1] demonstrated the need for turbulence models that are capable of predicting turbulent Prandtl and Schmidt numbers as part of the solution. They showed that an assumption of low Schmidt numbers can lead to predicted engine unstart, whereas high Schmidt numbers can lead to flame blowout.

Temperature and concentration fluctuations play a major role in combustion problems especially at high Mach numbers. Therefore, it is important to develop turbulence models that explicitly take into consideration, velocity, temperature, and concentration fluctuations. Such a development will make it possible to calculate the turbulent Prandtl and Schmidt numbers as part of the solution. The aim of this investigation is to develop the framework needed to accomplish this goal. This can be accomplished by deriving and modeling equations for the temperature (enthalpy) variance and its dissipation rate, and for the concentration variance and its dissipation rate. In the current investigation, emphasis will be placed on studying mixing without reactions.[2–4] For such flows, variable Prandtl numbers are not expected to play a major role in determining the flow. However, the choice of the Prandtl number is case dependent.

The approach employed is similar to that used in developing the k–ζ turbulence model.[5] Thus, relevant equations are derived from the exact Navier–Stokes, equations, and each individual correlation is modeled. This ensures that relevant physics is incorporated into the model. Because of the potential presence of a large number of species in a given problem, it is impractical to derive a concentration variance equation and a corresponding dissipation rate equation for each individual species. Instead, a multivariate β-probability density function (PDF) for the mass fractions is assumed.[6] This PDF is completely defined given the sum of the squares of mean mass fractions and the sum of their variances. Such an assumption reduces the turbulence model for concentration fluctuations to two equations: one governing the sum of variances of mass fractions and the other governing its dissipation rate.

Based on the preceding, the current turbulence model for multispecies, nonreacting flows consists of four equations: the k and ζ equations and two equations for the sum of variances of mass fraction and its dissipation rate. The model has no wall or damping functions. It is tensorially consistent and Galilean invariant and is coordinate system independent. The model is calibrated/validated using the data of Refs. 2–4.

Presented as Paper 2005-1099 at the AIAA 43rd Aerospace Sciences Meeting, Reno, NV, 10–13 January 2005; received 1 February 2005; revision received 25 August 2005; accepted for publication 6 September 2005.

*Research Assistant Professor, Mechanical and Aerospace Engineering. Member AIAA.
†Associate Professor, Mechanical and Aerospace Engineering. Associate Fellow AIAA.
‡Professor, Mechanical and Aerospace Engineering. Fellow AIAA.
§Associate Professor, Mechanical and Aerospace Engineering. Associate Fellow AIAA.

A k–ε-based model has been developed by Brinckman et al.[7] for scalar fluctuations. In their work the temperature variance equation and its dissipation rate were based on the work of Nagano and Kim[8] and Sommer et al.,[9] which, in turn, were based on the low-speed energy equation. The equations governing the scalar mass fraction and its dissipation rate are formally identical to those of the temperature variance and its dissipation rate and use the same model constants.

II. Formulation of the Problem

A. Governing Equations

The species conservation equation can be written as

$$\frac{\partial}{\partial t}(\rho Y_m) + \frac{\partial}{\partial x_j}(\rho u_j Y_m) = \frac{\partial}{\partial x_j}\left(\rho D \frac{\partial Y_m}{\partial x_j}\right) + \dot{\omega}_m \equiv S_Y \qquad (1)$$

where $\dot{\omega}_m$ is the production rate of species m. The preceding equation is used to derive the Favre-averaged equation

$$\frac{\partial}{\partial t}(\bar{\rho}\tilde{Y}_m) + \frac{\cdot\partial}{\partial x_j}(\bar{\rho}\tilde{u}_j\tilde{Y}_m) = \frac{\partial}{\partial x_j}\left(\bar{\rho} D \frac{\partial Y_m}{\partial x_j} - \overline{\rho Y_m'' u_j''}\right) + \overline{\dot{\omega}_m} \qquad (2)$$

an equation for the sum of the mass fraction variances σ_Y,

$$\sigma_Y = \sum_m \widetilde{Y_m''^2} \qquad (3)$$

and its dissipation rate ε_Y

$$\bar{\rho}\varepsilon_Y = \overline{\sum_m \rho D \left(\frac{\partial Y_m''}{\partial x_j}\right)^2} \qquad (4)$$

The exact equations governing σ_Y and ε_Y are given in the Appendix, whereas the modeled equations have the form

$$\frac{\partial}{\partial t}(\bar{\rho}\sigma_Y) + \frac{\partial}{\partial x_j}(\bar{\rho}\tilde{u}_j\sigma_Y) = \frac{\partial}{\partial x_j}\left[\bar{\rho}(D + C_{Y,1}D_t)\frac{\partial \sigma_Y}{\partial x_j}\right] + 2\sum_m \bar{\rho} D_t \left(\frac{\partial \tilde{Y}_m}{\partial x_j}\right)^2 - 2\bar{\rho}\varepsilon_Y \qquad (5)$$

when

$$D_t = 0.5\left(C_Y \frac{k\sigma_Y}{\varepsilon_Y} + \frac{\nu_t}{\sigma_h}\right) \qquad (6)$$

is the turbulent diffusion coefficient and ν_t is the turbulent kinematic viscosity

$$\frac{\partial}{\partial t}(\bar{\rho}\varepsilon_Y) + \frac{\partial}{\partial x_j}(\bar{\rho}\tilde{u}_j\varepsilon_Y) = \frac{\partial}{\partial x_j}\left[\bar{\rho}(D + C_{Y5}D_t)\frac{\partial \varepsilon_Y}{\partial x_j}\right] + 2\bar{\rho}\varepsilon_Y\left(\frac{1}{3}\frac{\partial \tilde{u}_i}{\partial x_i} + C_{Y2}b_{jk}\frac{\partial \tilde{u}_j}{\partial x_k}\right) + C_{Y3}\bar{\rho}k\sum_m \frac{\partial}{\partial x_j}\sqrt{\tilde{Y}_m''^2}\,\frac{\partial \tilde{Y}_m}{\partial x_j} + \bar{\rho}DC_{Y41}D_t\sum_m\left(\frac{\partial^2 \tilde{Y}_m}{\partial x_j \partial x_j}\right)^2 + \bar{\rho}D\frac{C_{Y42}}{\tau_Y}\sum_m \sqrt{\tilde{Y}_m''^2}\,\frac{\partial^2 \tilde{Y}_m}{\partial x_k \partial x_k} + \bar{\rho}D_t\frac{C_{Y6}}{\tau_Y}\sum_m\left(\frac{\partial \tilde{Y}_m}{\partial x_j}\right)^2 - C_{Y7}\bar{\rho}\frac{\varepsilon_Y}{\tau_Y} \qquad (7)$$

where

$$\tau_Y = \sigma_Y/\varepsilon_Y \qquad (8)$$

$$b_{jk} = \tau_{jk}/\bar{\rho}k + \tfrac{2}{3}\delta_{ij}, \qquad \tau_{jk} = -\overline{\rho u_j'' u_k''}, \qquad k = \tfrac{1}{2}\overline{u_i'' u_i''} \qquad (9)$$

The turbulent Schmidt number is defined as

$$Sc_t = \nu_t/D_t \qquad (10)$$

and σ_h, $C_Y - C_{Y7}$ are model constants given in Table 1.

Table 1 Model constants

Constant	Value
C_Y	0.065
C_{Y1}	1.0
C_{Y2}	0.095
C_{Y3}	−0.025
C_{Y41}	0.45
C_{Y42}	−1.0
C_{Y5}	1.0
C_{Y6}	0.5
C_{Y7}	0.78125
σ_h	0.5

Equation (6) merits further consideration. The modeling of D_T is patterned after the modeling of α_t, the thermal diffusivity.[10] It implies that the timescale for the mass fraction fluctuation is proportional to the average of τ_Y and τ_k, where τ_k is the timescale of velocity fluctuations. The model constant σ_h determines the diffusion coefficient in regions where the composition is essentially constant. It is generally believed that the turbulent Schmidt number should not exceed one. As a result, σ_h is chosen as 0.5.

B. Multivariate Beta Probability Distribution Function

The β-PDF used to reduce the number of variance of mass fraction equations and their corresponding dissipation-rate equations to two model equations [Eqs. (5) and (7)] irrespective of the number of species present is that developed by Girimaji.[6] It can be written as

$$F(Y_1, \ldots Y_m, \ldots) = \frac{1}{C(\beta_m)} \cdot \delta(1-s)\prod_{m=1}^{ncs} Y_m^{\beta_m - 1} \qquad (11)$$

$$s = \sum_m Y_m, \qquad C(\beta_m) = \prod_{m=1}^{ncs}\frac{\Gamma(\beta_m)}{\Gamma\left(\sum \beta_m\right)}$$

where Γ is the gamma function and δ is the Dirac delta function and ncs is the number of species present.

It can be shown that

$$\beta_m = \tilde{Y}_m[(1 - S_Y)/\sigma_Y - 1] \equiv \tilde{Y}_m(\sigma - 1) \qquad (12)$$

where

$$S_Y = \sum_m (\tilde{Y}_m)^2 \qquad (13)$$

Further, it follows from the preceding that

$$\overline{Y_k'' Y_m''} = (\tilde{Y}_m\delta_{km} - \tilde{Y}_m\tilde{Y}_k)/\sigma \qquad (14)$$

where δ_{mk} is the Kronecker delta, which is equal to 1 when $k = m$ and zero otherwise.

As is seen from Eq. (14), all variances and covariances are determined from the species conservation equations, Eq. (2), whereas σ_Y follows from Eqs. (5) and (7).

C. Numerical Procedure

A modification of REACTMB,[11] a code that has been developed at North Carolina State University over the past several years, was employed in this investigation. It is a general-purpose parallel Navier–Stokes solver for multicomponent multiphase reactive flows at all speeds. It employs a second-order essentially nonoscillatory upwind method based on the low-diffusion flux-splitting scheme of Edwards[12] to discretize the inviscid fluxes while central differences are employed for the viscous and diffusion terms. Planar relaxation is employed, and the code is parallelized using domain decomposition and message-passing strategies.

D. Model Constants

The model constants are derived by using the experiments of Ref. 2. The general procedure requires selecting a station where flow measurements are available and trying to determine the constants that give the best fit for the flow properties at the selected station.

III. Results and Discussion

The predictions of the present theory are compared with two sets of experiments conducted at two different facilities. In the experiments of Cutler et al.,[2,3] a coaxial nozzle was designed to produce two uniform coaxial jets at the exit. The center flow consists of 95% He, 5% O_2 by volume at a Mach number $M = 1.8$, while the outer flow is that of air at $M = 1.8$. A schematic of the experimental setup is shown in Fig. 1. Velocity, pitot pressure, composition, total temperature, and growth rate were measured.

The grid employed is that used in Ref. 3. The fine grid consists of 188,080 cells and is decomposed into 13 blocks for parallel computing. The intermediate grid deletes every other point in the axial direction but maintains the number of grids in the radial direction. As is seen in the following, the solution is grid independent. All of the results are based on the fine grid. Using a three-dimensional code to calculate axisymmetric flows invariably requires an excessive amount of calculations.[13] Because of this, an axisymmetric version of REACTMB is developed. All results presented here employ the axisymmetric code.

The results will be presented in two stages. The first is devoted to flows in which the turbulent Schmidt number is assumed constant, whereas the second will employ the newly developed variable turbulent Schmidt-number model. As was done in Refs. 2 and 3, the range of r in the plots is truncated to show more clearly the region of interest. In general, good agreement is indicated beyond the range indicated in the figures.

For the constant Schmidt-number case, the turbulent diffusion coefficient is determined by

$$D_t = \nu_t / Sc_t \tag{15}$$

Figures 2–6 compare calculations and measurements for the He–O_2 mass fraction, velocity, pitot pressure, temperature, and spreading rate. The calculations were carried out for turbulent Schmidt numbers of 1.0, 0.9, and 0.6 and a value of 0.89 for the turbulent Prandtl number.

Figure 2 compares computed and measured mass fractions at selected stations. As is seen from the figure, a Schmidt number of 1.0 gives better agreement with experiment. Note also that there is

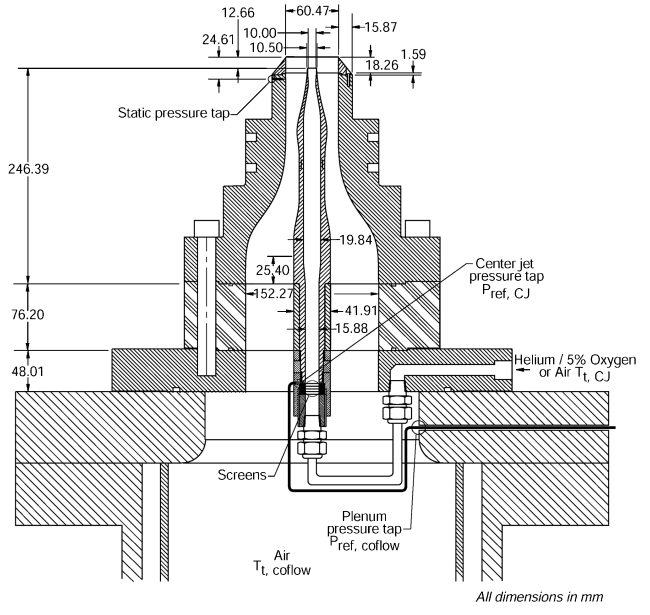

Fig. 1 Schematic of the experimental setup.[2]

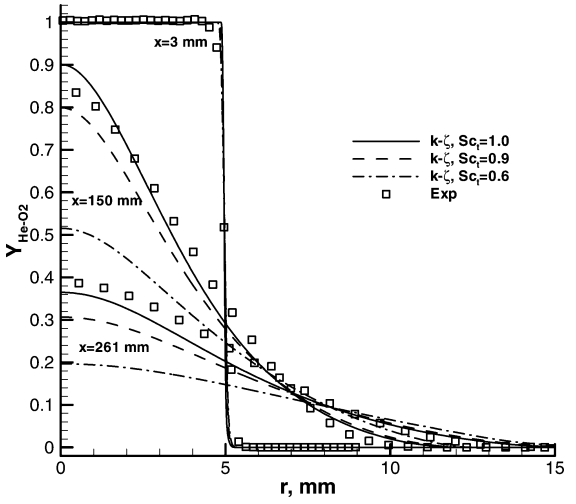

Fig. 2 Comparison of computed and measured He–O_2 mass fraction.[2]

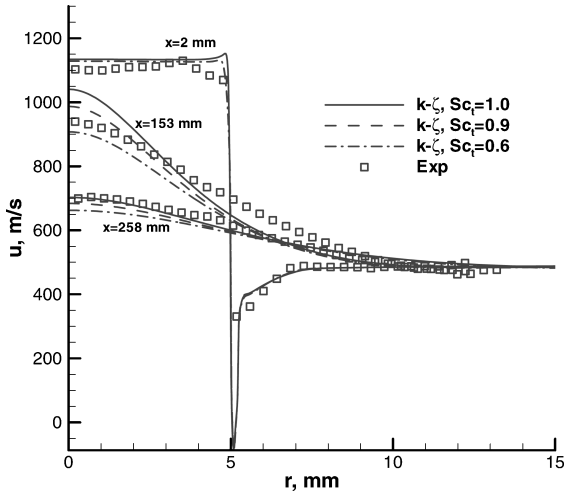

Fig. 3 Comparison of computed and measured velocities.[2]

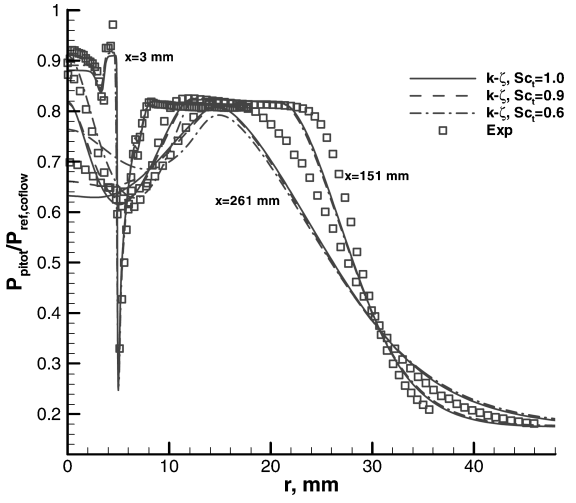

Fig. 4 Comparison of computed and measured pitot pressure.[2]

no discontinuity in the slope of the mass fraction for any of the cases considered as was noted in Ref. 13, where the k–ω model was used. As is seen from the figure, calculated results are rather sensitive to the turbulent Schmidt number near the axis; a reduced value of the mass fraction is noted at the lower Schmidt number because of enhanced diffusion.

The mean velocity is shown in Fig. 3. At $x = 2$ mm, the velocity profile is a result of merging of the coflow nozzle inner-surface

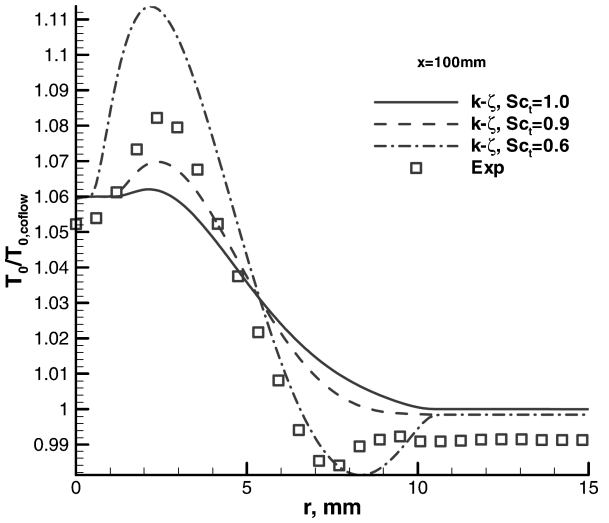

Fig. 5 Comparison of computed and measured total temperature.[2]

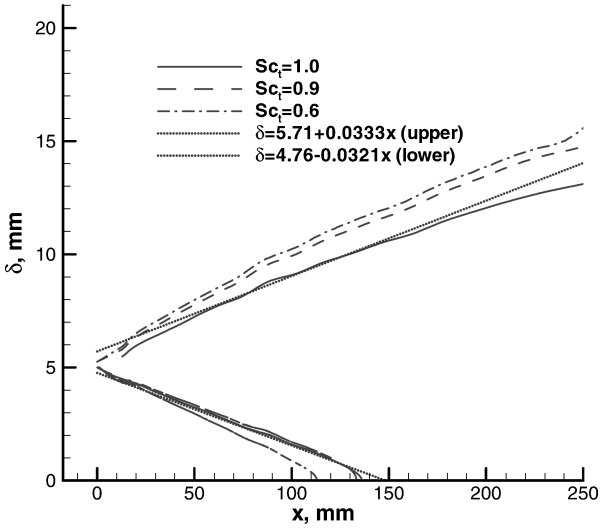

Fig. 6 Growth rate of mixing layer.[2]

boundary layer with the region of separation at the lip and the shock wave emanating from the lip. Downstream, the calculated velocity is in good agreement with the measurements and is not sensitive to the Schmidt number.

The pitot pressure is shown in Fig. 4. As is seen from $x = 3$ mm station, there is a layer with reduced pitot pressure at the boundary between the center jet and the coflow. Downstream, the center jet spreads with the pressure near the axis falling and then rising in the wake of the nozzle lip. The figure shows that the pitot pressure is somewhat sensitive to the Schmidt number near the axis. This behavior is a result of the behavior of the He–O_2 mass fraction indicated in Fig. 2.

The measured and calculated total temperature is shown in Fig. 5. Measurements[2,3] indicate that the gas supply temperature varied substantially from run to run. Because of this, it was recommended that calculations employ the experimentally measured temperature for that run and not the average temperature over many runs as was done for other parameters. A value of $T_{0,\,\mathrm{coflow}} = 300 \pm 6$ was indicated in Ref. 2. A value of 300 is used in the present calculations. When the probe errors (of the order of 1%) are taken into consideration, it is seen that agreement with experiment is acceptable. However, results are Schmidt-number dependent.

Figure 6 compares the computed and measured growth rate of the mixing region. This region is defined by $Y_{\mathrm{He-O_2}}$ ranging from 0.99 to 0.01. The experimental data were fitted by two straight lines:

$$\delta = 5.71 + 0.0333x, \qquad Y_{\mathrm{He-O_2}} = 0.01$$

$$\delta = 4.76 - 0.0321x, \qquad Y_{\mathrm{He-O_2}} = 0.99$$

As is seen from the figure, the growth rate is overpredicted for both $Sc_t = 0.6$ and 0.9 and well predicted for $Sc_t = 1.0$.

The preceding results provide the needed justification for the development of a turbulence model that predicts the turbulent Schmidt number as part of the solution.

For the case where the turbulent Schmidt number is variable, the turbulent diffusion coefficient, Eq. (6), is calculated as part of the solution. The turbulent Schmidt number follows from the relation given by Eq. (10). As can be seen from Eq. (6), the turbulent Schmidt number assumes a constant value in regions where $\sigma_Y \to 0$, that is, in regions where mass fraction fluctuations are negligible. The choice of σ_h determines the constant value specified by the user. In this work σ_h is chosen as 0.5. Thus, $Sc_t \to 1$ when $\sigma_Y \to 0$.

A contour plot of turbulent Schmidt number is shown in Fig. 7. As is seen from the figure, the turbulent Schmidt number is small, as low as 0.16, along the boundary separating the two coaxial jets resulting in enhanced diffusion and mixing. Figure 8 shows the growth rate of the mixing region. As is seen from the figure, good agreement with experiment is indicated.

Figure 9 compares the computed and measured mass fractions on the intermediate and fine grid. As is seen from the figure, the

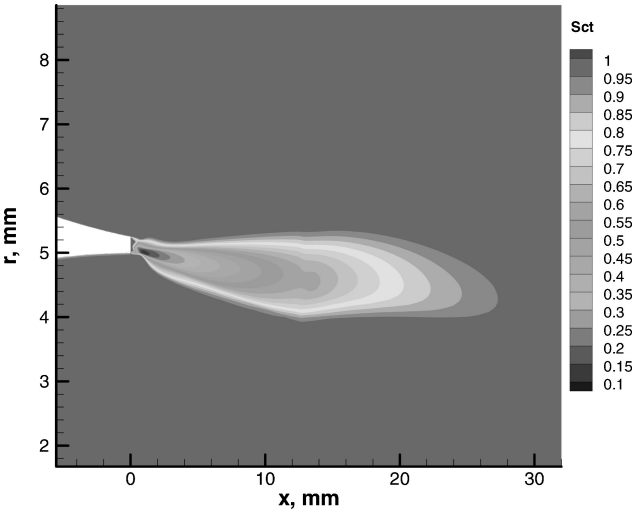

Fig. 7 Contour plot of the turbulent Schmidt number.

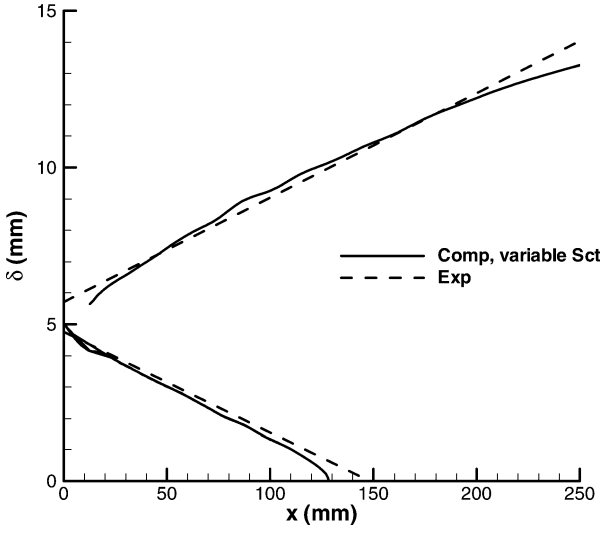

Fig. 8 Growth rate of mixing layer (variable Sc_t).[2]

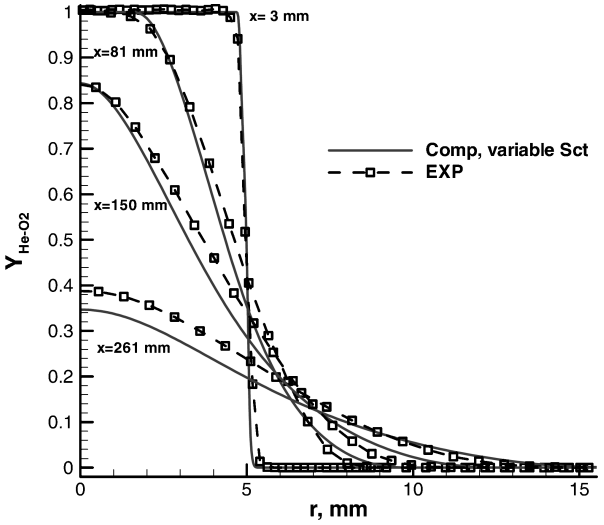

Fig. 9 Comparison of computed and measured He–O_2 mass fraction.[2]

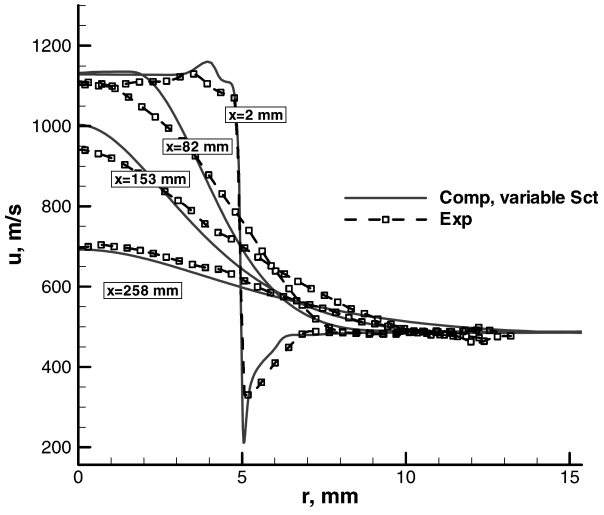

Fig. 10 Comparison of computed and measured velocities.[2]

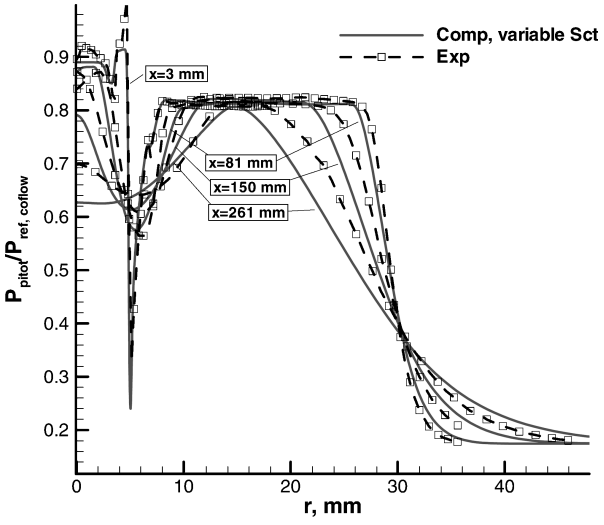

Fig. 11 Comparison of computed and measured pitot pressure.[2]

solution is grid independent. The mass fraction is the property most affected by the local turbulent Schmidt number. Overall agreement with experiment is quite satisfactory. When comparing the results with those for the constant Schmidt number of one at the 150-mm station, it is noticed that the variable Schmidt-number results are in better agreement with experiment near the axis because the local Schmidt number is small The good agreement with experiment is responsible for the good prediction of spreading rate indicated in Fig. 8.

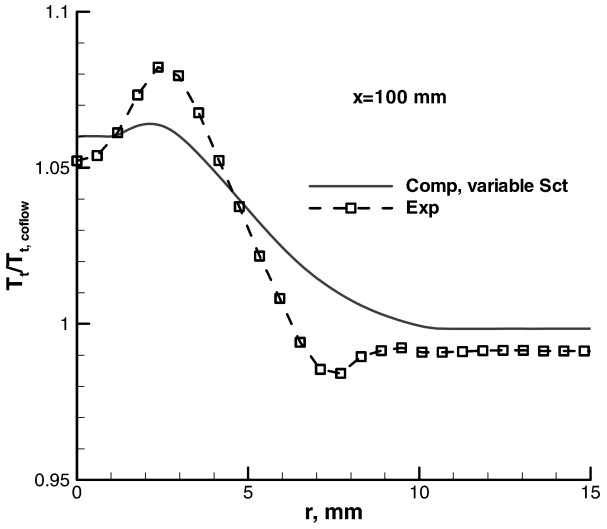

Fig. 12 Comparison of computed and measured total temperature.[2]

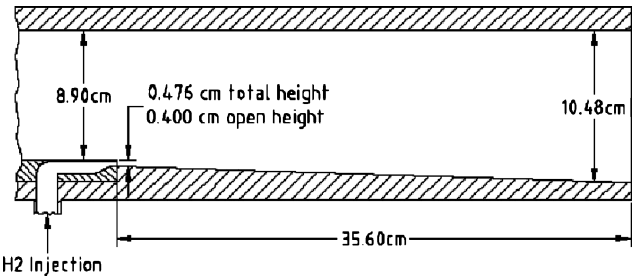

Fig. 13 Schematic of experiment.[4]

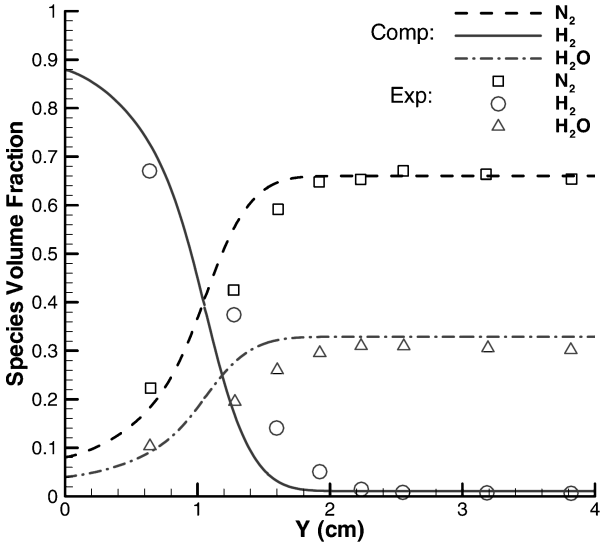

Fig. 14 Composition profiles, mixing case ($Pr_t = 0.9$, $Sc_t = 0.5$), k–ζ model.[4]

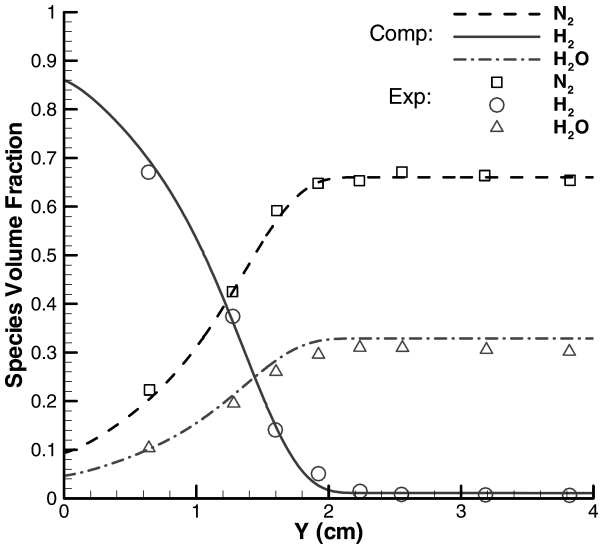

Fig. 15 Composition profiles, mixing case ($Pr_t = 0.5$, $Sc_t = 0.5$), k–ζ model.[4]

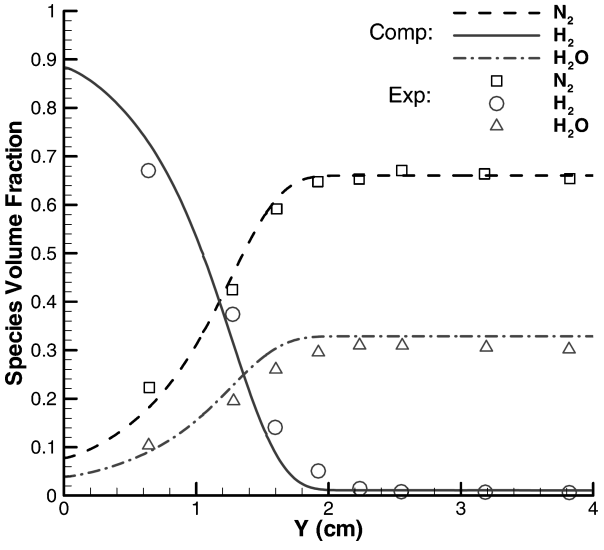

Fig. 16 Composition profiles, mixing case, variable Sc_t, $Pr_t = 0.5$, k–ζ model.[4]

Figure 10 compares predicted and measured velocities. As is seen from the figure, comparisons for $x = 82$ and 150 mm are not in good agreement with experiment. The velocity is overpredicted near the axis and underpredicted away from the axis. Figure 11 compares the calculated pitot pressure. It is seen that computations underpredict measurements in both inner and outer regions and are somewhat similar to the constant turbulent Schmidt-number results. It is not clear why such discrepancies exist for velocity and pressure. In the present calculations, we assumed that measured mean total pressure and total temperature were given at the nozzle inlet. As was mentioned earlier, it was indicated[2,3] that the gas supply temperature varied substantially from run to run. It is possible that the discrepancy is a result of variation in supply temperature. Because similar behavior in velocity and pressure prediction is noted for both constant and variable Schmidt-number calculations, it is believed that the discrepancy is not turbulent Schmidt number related.

Figure 12 compares measured and computed total temperature. The rise in T_0 is underpredicted while the dip in the total temperature is not predicted similar to the $Sc_t = 1.0$ results indicated in Fig. 5. When the probe error is taken into consideration, it is deemed that agreement with experiment is fair.

The predictions using the variable Schmidt-number model with the same set of model constants are compared next with the experiments of Burrows and Kurkov.[4] A schematic of the experiment is shown in Fig. 13. Hydrogen was injected into the test section through a nickel injector parallel to the vitiated main flow at Mach 1 and atmospheric pressure. Hydrogen was heated in a storage heater so that the total temperature of the hydrogen flowing in the slot could be varied from 200 to 800 K. The mixing case used vitiated nitrogen for the main flow.

Two grids, each consisting of 15 blocks, were employed in the calculations. The first grid has 86,643 cells, whereas the second has 104,428 cells. Refinements were made in the blocks where mixing of the two streams took place. Both hydrogen and vitiated nitrogen nozzles are included. It was necessary to iterate on the inlet conditions of both nozzles to arrive at the stipulated conditions at the exit of each nozzle.

It was indicated in Ref. 14 that results were sensitive to both Sc_t and the turbulent Prandtl number Pr_t. Because we are assessing the role of a variable Sc_t formulations, initial calculations focused on finding the best combination of constant Sc_t and Pr_t that best predicted the mixing mole fraction distributions.

All results presented here employ the fine grid. Figures 14 and 15 compare the role of Pr_t for $Sc_t = 0.5$ using the k–ζ model model.[5] These figures show profiles of species volume fractions 35.6 cm downstream of the hydrogen injector. It is seen from these figures that $Sc_t = Pr_t = 0.5$ gives the best fit. Because of this, all subsequent calculations assume $Pr_t = 0.5$. Figure 16 compares mole fraction predictions with experiment for a variable Sc_t. It is seen that good agreement is indicated. Figure 17 shows a contour of Sc_t and the extent of mixing of the two streams.

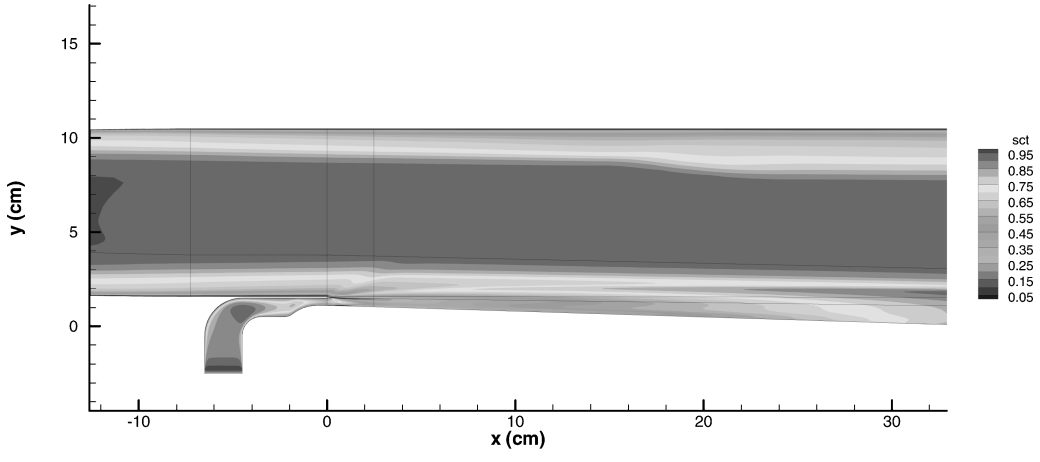

Fig. 17 Contour of turbulent Schmidt number, mixing case.

IV. Conclusions

A new approach has been developed for calculating the turbulent Schmidt number as part of the solution. The approach is based on a two-equation model for the sum of the variances of the mass fractions σ_Y and its dissipation rate ε_Y. The approach used in developing the new model equations follows the approach employed in deriving the k–ζ turbulence model. Thus all correlations that appear in the exact equations governing σ_Y and ε_Y are modeled to ensure the incorporation of relevant physics into the model equations. The resulting set of equations is tensorially consistent and Galilean invariant and is coordinate system independent. Moreover, the model has no wall or damping functions.

The new formulation is used first to model the mixing experiments of Cutler et al.[2,3] Calculations were carried out first for three constant turbulent Schmidt numbers of 1.0, 0.9, and 0.6, and the result demonstrates the need for a variable turbulent Schmidt-number formulation. The predictions of the new approach show that properties that are highly dependent on the turbulent Schmidt number such as mass (mole) fractions and the growth of the mixing region are well predicted. Discrepancies in velocity and pressure predictions are noted. It is believed that they can be traced to supply gas temperature, which varied from one set of experiment to the next.

The results show that along the boundaries separating the two streams local turbulent Schmidt numbers can be as low as 0.16 resulting in enhanced diffusion in that region.

The model performed well when the Burrows and Kurkov[4] are considered. This experiment further demonstrates that the turbulent Prandtl number is case dependent. This demonstrates the need for turbulence models in which both Schmidt and Prandtl numbers are calculated as part of the solution.

Finally, the present model represents an important building block in arriving at a turbulence model suited for predicting high-speed reacting flows.

Appendix: Governing Equations for σ_Y and ε_Y

Exact equations for mass fraction variance and its dissipation rate are as follows:

$$\frac{\partial}{\partial t}(\bar{\rho}\sigma_Y) + \frac{\partial}{\partial x_j}(\bar{\rho}\tilde{u}_j\sigma_Y) = \frac{\partial}{\partial x_j}\left(\bar{\rho}D\,\frac{\partial \sigma_Y}{\partial x_j} - \sum_m \overline{\rho u_j'' Y_m''^2}\right) + 2\sum_m\left[-\overline{\rho u_j'' Y_m''}\frac{\partial \tilde{Y}_m}{\partial x_j} - \bar{\rho}D\left(\overline{\frac{\partial Y_m''}{\partial x_j}}\right)^2 + \overline{\dot{\omega}_m Y_m''}\right] \tag{A1}$$

$$\rho\frac{D}{Dt}\varepsilon_Y + \sum_m\left[\overline{2\rho D\frac{\partial Y_m''}{\partial x_k}\frac{\partial Y_m''}{\partial x_j}}\cdot\frac{\partial \tilde{u}_j}{\partial x_k} + \overline{2\rho D\frac{\partial u_j''}{\partial x_k}\frac{\partial Y_m''}{\partial x_k}}\cdot\frac{\partial \tilde{Y}_m}{\partial x_j} + \overline{\rho D u_j''\frac{\partial}{\partial x_j}\left(\frac{\partial Y_m''}{\partial x_k}\right)^2} + \overline{2\rho D u_j''\frac{\partial Y_m''}{\partial x_k}}\frac{\partial^2 \tilde{Y}_m}{\partial x_j \partial x_k} + \overline{2\rho D\frac{\partial u_j''}{\partial x_k}\frac{\partial Y_m''}{\partial x_j}\frac{\partial Y_m''}{\partial x_k}}\right]$$

$$= \sum_m \overline{2\rho D\frac{\partial Y_m'''}{\partial x_k}\frac{\partial}{\partial x_k}\left[\frac{S_Y'}{\rho} - \frac{1}{\rho}\frac{\partial}{\partial x_j}\overline{(\rho u_j'' Y_m'')}\right]} \tag{A2}$$

with

$$S_Y' = \frac{\partial}{\partial x_j}\left(\rho D\frac{\partial Y_m''}{\partial x_j}\right) + \dot{\omega}_m' \tag{A3}$$

Acknowledgments

The authors from North Carolina State University acknowledge partial support under NASA Grant NAG-1-03030 and Air Force Contract FA9101-04-C-0015.

References

[1]Eklund, D. R., Baurle, R. A., and Gruber, M. R., "Numerical Study of a Scramjet Combustor Fueled by an Aerodynamic Ramp Injector in Dual-Mode Combustion," AIAA Paper 2001-0379, Jan. 2001.

[2]Cutler, A. D., Diskin, G. S., Danehy, P. M., and Drummond, J. P., "Fundamental Mixing and Combustion Experiments for Propelled Hypersonic Flight," AIAA Paper 2002-3879, July 2002.

[3]Cutler, A. D., Carty, A. A., Doemer, S. E., Diskin, G. S., and Drummond, J. P., "Supersonic Coaxial Jet Flow Experiment for CFD Code Validation," AIAA Paper 99-3588, July 1999.

[4]Burrows, M. C., and Kurkov, A. P., "Analytical and Experimental Study of Supersonic Combustion of Hydrogen in a Vitiated Airstream," NASA TM X-2828, Sept. 1973.

[5]Robinson, D. F., and Hassan, H. A., "Further Development of the k–ζ (Enstrophy) Turbulence Closure Model," *AIAA Journal*, Vol. 36, No. 10, 1998, pp. 1825–1833.

[6]Girimaji, S. S., "A Simple Recipe for Modeling Reaction-Rates in Flows with Turbulent-Combustion," AIAA Paper 91-1792, June 1991.

[7]Brinckman, K. W., Kenzakowski, D. C., and Dash, S. M., "Progress in Practical Scalar Fluctuation Modeling for High-Speed Aeropropulsive Flows," AIAA Paper 2005-0508, Jan. 2005.

[8]Nagano, Y., and Kim, C., "A Two-Equation Model for Heat Transport in Wall Turbulent Shear Flows," *Journal of Heat Transfer*, Vol. 110, Aug. 1988, pp. 583–589.

[9]Sommer, T. P., So, R. M. C., and Zhang, H. S., "Near-Wall Variable-Prandtl Number Turbulence Model for Compressible Flows," *AIAA Journal*, Vol. 31, No. 1, 1993, pp. 27–35.

[10]Xiao, X., Edwards, J. R., Hassan, H. A., and Gaffney, R. L. Jr., "Role of Turbulent Prandtl Number on Heat Flux at Hypersonic Mach Numbers," AIAA Paper 2005-1098, Jan. 2005.

[11]Edwards, J. R., "Advanced Implicit Algorithms for Finite-Rate Hydrogen-Air Combustion Calculations," AIAA Paper 96-3129, June 1996.

[12]Edwards, J. R., "A Low Diffusion Flux Splitting Scheme for Navier–Stokes Calculations," *Computers and Fluids*, Vol. 26, No. 6, 1997, pp. 635–659.

[13]Cutler, A. D., and White, J. A., "An Experimental and CFD Study of a Supersonic Axial Jet," AIAA Paper 2001-0143, Jan. 2001.

[14]Parent, B., and Sislian, J. P., "Validation of Wilcox k–ω Model for Flows Characteristic to Hypersonic Airbreathing Propulsion," *AIAA Journal*, Vol. 42, No. 2, 2004, pp. 261–270.

A. Karagozian
Associate Editor